ACS APPLIED MATERIALS & INTERFACES

Research Article

www.acsami.org

Electromagnetic Interference (EMI) Transparent Shielding of Reduced Graphene Oxide (RGO) Interleaved Structure Fabricated by Electrophoretic Deposition

Sanghoon Kim,[†] Joon-Suk Oh,[§,∥] Myeong-Gi Kim,[‡] Woojin Jang,[§] Mei Wang,[†] Youngjun Kim,[§] Hee Won Seo,[§] Ye Chan Kim,[†] Jun-Ho Lee,[†] Youngkwan Lee,[⊥] and Jae-Do Nam*[,†,§,∥]

[†]Department of Energy Science, Sungkyunkwan University, Suwon, Gyeonggi-Do 440-746, Republic of Korea (South Korea)

[‡]LCR Product Development Group, Samsung Electro-Mechanics, Suwon, Gyeonggi-Do 443-743, Republic of Korea (South Korea)

[§]Department of Polymer Science and Engineering, Sungkyunkwan University, Suwon, Gyeonggi-Do 440-746, Republic of Korea (South Korea)

[∥]SKKU Advanced Institute of Nanotechnology (SAINT), Sungkyunkwan University, Suwon, Gyeonggi-Do 440-746, Republic of Korea (South Korea)

[⊥]Department of Chemical Engineering, Sungkyunkwan University, Suwon, Gyeonggi-Do 440-746, Republic of Korea (South Korea)

ABSTRACT: Here we introduce the electromagnetic shielding effectiveness (SE) of reduced graphene oxide (RGO) sheets interleaved between polyetherimide (PEI) films fabricated by electrophoretic deposition (EPD). Incorporating only 0.66 vol % of RGO, the developed PEI/RGO composite films exhibited an electromagnetic interference shielding effectiveness (EMI SE) at 6.37 dB corresponding to ∼50% shielding of incident waves. Excellent flexibility and optical transparency up to 62% of visible light was demonstrated. It was achieved by placing the RGO sheets in the localized area as a thin film (ca. 20 nm in thickness) between the PEI films (ca. 2 μm) to be an interleaved and alternating structure. This unique interleaved structure without any delamination areas was fabricated by a successive application of cathodic and anodic EPD of both RGO and PEI layers. The EPD fabrication process was ensured by an alternating deposition of the quarternized-PEI drops and RGO, each taking positive and negative charges, respectively, in the water medium. We believe that the developed facile fabrication method of RGO interleaved structure with such low volume fraction has great potential to be used as a transparent EMI shielding material.

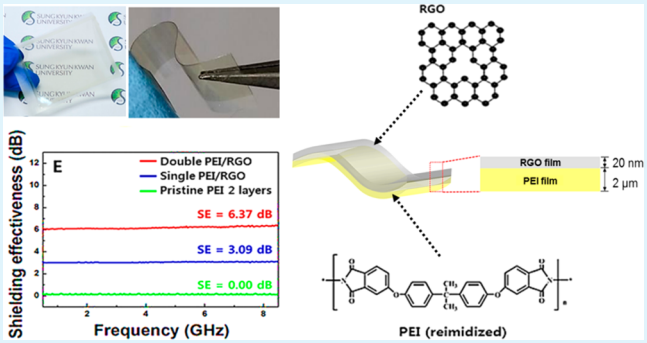

KEYWORDS: *RGO, EPD, transparent, flexible, conductive, EMI, SE*

INTRODUCTION

Recently, radio frequency (RF) emission has become a serious concern in the advent of rapid development of various electronic devices.[1,2] Electromagnetic emission at high frequencies often interferes with other electronics to cause malfunctions and it has also raised human health issues.[3] Thus, electromagnetic interference (EMI) shielding is considered a significant issue in our daily lives. The EMI shielding is particularly difficult in areas where visual observation is needed, e.g., observation windows,[3] electronic displays,[4] mobile communication devices,[5,6] etc. For those applications, various transparent EMI shielding materials have been investigated including carbon nanotubes (CNT),[7] graphene,[8] metal doped ZnO,[9] polyaniline,[10] poly(3,4-ethylenedioxythiophene (PEDOT),[11] etc. As a form of thin films, the EMI shielding effectiveness (SE) of transparent materials have been reported as, for example, 2.27 dB (frequency range of 2.2−7 GHz) for monolayer CVD graphene,[12] 8 dB (0−16 GHz) for polyaniline,[13] and 6.5 dB (30 MHz−1.5 GHz) for Al doped ZnO.[14]

Particularly, graphene is considered as a promising material for the development of transparent EMI shielding due to optical, excellent electronic, mechanical, and thermal properties subsequently allowing various applications in transparent conducting electrodes, photovoltaic devices, sensors, and transistors.[15−18] For the EMI performance to be increased in graphene systems, the amount of graphene should be increased. And it is usually difficult to increase the amount of graphene while maintaining transparency because the graphene is usually mixed with matrix materials in a bulk form. Several bulk mixtures of graphene composites have been reported, for example, as ∼21 dB for graphene/epoxy (8.8 vol %),[19] ∼19 dB

Received: June 18, 2014
Accepted: September 19, 2014
Published: September 19, 2014

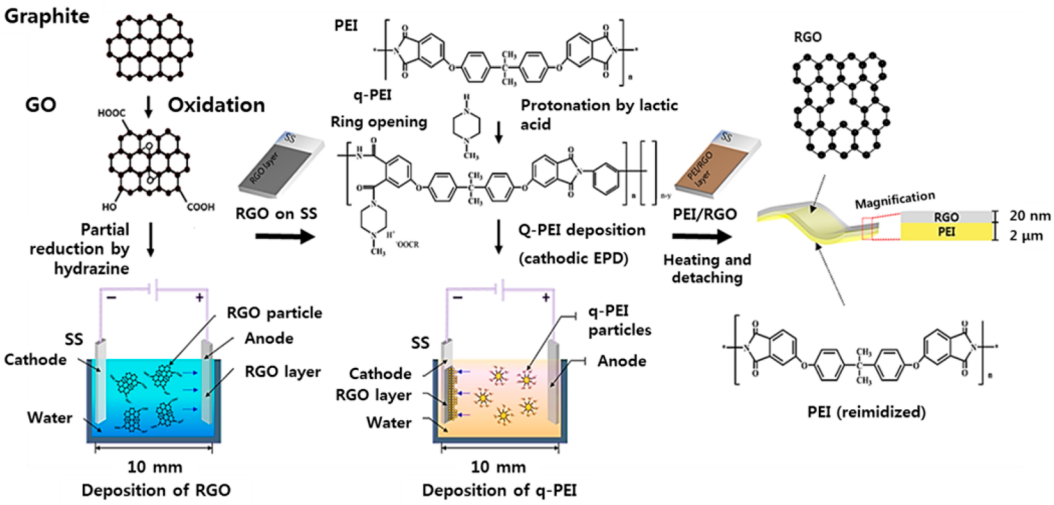

Figure 1. Schematic of alternating anodic and cathodic EPD process, where the negatively charged RGO sheets are deposited on positive electrode (anodic EPD),[35] and the positively charged q-PEI drops on negative electrode (cathodic EPD).[35]

for graphene/polystyrene (5.6 vol %),[20] and ~30 dB for graphene/polymethylmethacrylate (4.2 vol %).[21] In these high content composite systems in the bulk mixture, transparency cannot be achieved and the high viscosity usually makes composite fabrication difficult. Thus, an efficient fabrication method for transparent EMI shielding films remains a challenge. In this sense, an interleaved graphene/polymer structure composed of thin layers of graphene sheets may be an ideal architecture for the development of EMI shielding in the areas where transparency should be guaranteed. It should be mentioned that the thin graphene layer ensures visual transparency in the through-thickness direction and the electrical percolation in the in-plane direction.

There are various methods of fabricating graphene thin films, such as spin-coating,[22] vacuum-filtration,[23,24] chemical vapor deposition (CVD),[25,26] etc. Recently, the EPD process has been introduced for the fabrication of graphene sheets.[27,28] Compared with other fabrication methods, the EPD process has many advantages specifically in high deposition/production rates, excellent purity control, wide range of thickness control, and deposition on complex shaped substrates, including the potential to infiltrate porous substrate. Because the exfoliated graphene oxide (GO) takes a negative charge,[28] EPD may allow anodic EPD of GO sheets from the stabilized GO suspension on the surface of conductive substrates. Subsequently, the GO sheets can be reduced either chemically or thermally to become a RGO, which could restore the electrical conductivity.[29] In the EPD process, the GO (or RGO) sheets are deposited on a metal substrate aligned well in the in-plane direction and, consequently, give a high electrical conductivity. The aligned thin graphene layer may well give excellent EMI shielding characteristics along with transparency. It should be also noted that the strong electrophoretic squeezing force, which is usually generated in the EPD process, could facilitate cohesive flocculation of graphene sheets in the in-plane direction, desirably eliminating use of binder materials.[30]

The RGO interleaved structure between polymer layers was expected to be good for EMI shielding, while maintaining the transparency. For this reason, the polymer with a good transparency was required. In this sense, PEI was considered as an organic layer, which is also available for EPD.[31]

Herein we report the interleaved multilayer structure of the RGO/polymer composites film, fabricated by the alternating cathodic and anodic EPD process. The electrostatic surface charges of RGO sheets were controlled to ensure a stable aqueous mixture and the appropriate interleaved RGO/polymer structure. The EMI-shielding performance and optical characteristics of the multilayered RGO/polymer was investigated.

EXPERIMENTAL SECTION

Materials. Natural graphite flakes, sulfuric acid (95–97%, H_2SO_4), phosphoric acid (85%, H_3PO_4), chloric acid (HCl), hydrogen peroxide (30%, H_2O_2), potassium permanganate ($KMnO_4$), *N*-methylpyrrolidone (NMP), acetophenone, 1-methylpiperazine, lactic acid (50%), and hydrazine (35%, N_2H_4) were purchased from Sigma-Aldrich. Polyetherimide (PEI, ULTEM 1000) was purchased from Quadrant Co., Ltd. (Korea).

Preparation of RGO Suspension[30] and PEI Emulsion.[31] For the preparation of the GO suspension, H_2SO_4 (360 mL) and H_3PO_4 (40 mL) were mixed at a ratio of 9:1. This mixture was mixed with the graphite flakes (10 g) while stirring for 1 h and, then, $KMnO_4$ (40 g) was added and the solution was heated up to 50 °C.[32] This oxidative reaction of graphite was carried out for 2 h. After the reaction was over, deionized water (DI-water) and H_2O_2 at a ratio of 9:1 was added to the mixture and the solution was stirred for about 30 min in order to remove impurities inside. Afterward, the oxidized graphite (GrO) flakes were collected by filtration, and the filtrate was washed several times with the mixture of DI-water and HCl at a ratio of 9:1. The GrO (0.1 g) was added to DI-water (100 mL) and exfoliated by sonication for 4 h, followed by centrifugation of the suspension for 15 min at 4000 rpm to derive pure GO suspension.[29,32]

For the preparation of the RGO suspension, the mixture of N_2H_4 (10 mL)/DI-water (40 mL) solution was slowly added to the GO suspension for 1 h at 5 °C in order to prevent the agglomeration of RGO.[29] Afterward, the mixture was heated to 100 °C in an oil bath for 30 min, resulting in a stable RGO suspension.

For the preparation of the quarternized PEI (q-PEI) emulsion, acetophenone (20.6 g) and NMP (165.3 g) were mixed. The mixture was added to the PEI pallets (80 g), then put into an oil bath and heated up to 90 °C, and the reaction was carried out for 4 h with gentle stirring in the N_2 condition. After the PEI pallets were completely dissolved in the solvent, the mixture of acetophenone (62 g) and 1-methylpiperazine (18.9 g) was added slowly within 2 h to the PEI solution with vigorous stirring. When the addition was completed, the solution was heated up to 110 °C and this quarternization reaction

was carried out for 2 h and 30 min. Afterward, the mixture of acetophenone (5.96 g) and lactic acid (1.48 g) was added to the q-PEI solution, and then DI-water (80 mL) was slowly added to the solution to give a milky emulsion.[31]

Fabrication of PEI/RGO Bilayer Film by EPD. Two stainless steel (SS) electrodes were immersed into the RGO suspension with a distance at 1 cm. During anodic EPD, DC voltage was controlled in the range of 5−7 V, and the deposition time was controlled between 5 s and 10 min. After the deposition was over, the RGO film was washed with DI-water and deposited on the metal electrode to remove remaining impurities. Afterward, sample was dried at room temperature for 24 h. The thickness of the deposited RGO film was controlled as ca. 20 nm.

The q-PEI was subsequently deposited on the fabricated RGO film by the cathodic EPD process, where the q-PEI drops take a positive charge, due to acid-protonated amine groups on the drop surface.[31] The RGO-coated SS electrode was immersed in the q-PEI emulsion with an interval distance of 1 cm from a counter electrode (SS). Applying (+) potential on the RGO electrode, the deposition time and voltage were fixed at 5 min and 2 V, respectively.[31] After EPD, the q-PEI coated RGO film steel was immediately withdrawn from the q-PEI emulsion, and washed with DI-water, and dried in air at room temperature for 1 h. Then the film was replaced into a vacuum oven annealing over 250 °C for 3 h, when the remaining solvent was removed and the deposited q-PEI was converted to PEI throughout the reimidization reaction.[31]

As schematically shown in Figure 1, the RGO particles migrate toward the positive electrode (anodic EPD), when a DC voltage was applied due to their negative charge attributed by remaining carboxylic groups on edge of RGO.[33−35] On the contrary, the q-PEI particles take positive charges, and subsequently migrate to negatively charged electrode (cathodic EPD).[32] In this study, a bilayer [RGO/PEI] film was fabricated by a series deposition of RGO (anodic EPD) and q-PEI (cathodic EPD) under the controlled concentrations and deposition conditions of time and voltage.

The density of RGO (ρ_f) and PEI (ρ_m) was measured by using pycnometer (AccuPyc1330) to calculate the volume fractions of single- and double-PEI/RGO composite films. The two-thirds space of cup in the picnometer was filled by either RGO powders or PEI pellets and then the helium gas was injected into the cup during the measurement. The volume fraction of RGO was calculated using the following equation:[36]

$$\nu_f = \frac{\rho_m \rho_f}{(\rho_m - \rho_f)W_f + \rho_f} \quad (1)$$

where ν_f is the volume fraction, W_f is the filler's weight fraction, ρ_m is the density of PEI (ca. 1.25 g/cm^3), and ρ_f is the density of the RGO (ca. 2.32 g/cm^3).

Measurement of EMI Shielding. Fabricated films were cut into donut-shaped strips of size 7 mm outer diameter and 3 mm inner diameter. The schematic of the waveguide measurement device for the measurement of EMI SE is shown in Figure 2. Two waveguide-to-coaxial adapters and a vector network analyzer (Agilent E5071A) were used to measure the scattering parameter (S21) between the two waveguide-to-coaxial adapters connected face to face, where specimens were placed on the commissure of two waveguide-to-coaxial adapters. The measurement was carried out over a frequency range of 0.5−8.5 GHz. The pristine PEI film without RGO was also measured and used as a SE reference.

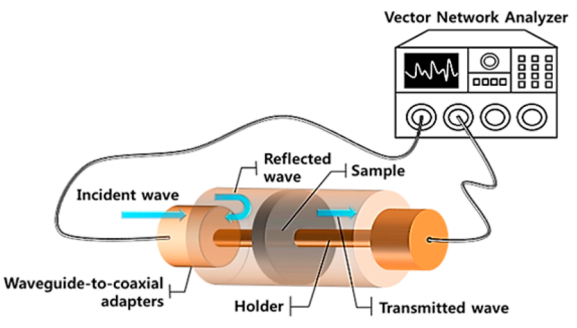

Figure 2. Schematic of two waveguide-to-coaxial adapters and a vector analyzer was used to measure the EMI SE of RGO over a frequency range of 0.5−8.5 GHz.

Characterization. The surface morphology of PEI coated RGO film was examined by field emission scanning electron microscopy (FE-SEM, SUPRA 55VP, Germany). The cross-sectional morphology of specimens was observed by transmission electron microscopy (TEM, JEM1010). Raman spectroscopy (WITec, alpha 300 M) with a wavelength source of 532 nm was used. Transmittances of prepared specimens were measured by UV−visible-near infrared spectroscopy (UV−vis/NIR, Cary 5000). The sheet resistance was measured by a four-point probe method (Keithley) at room temperature. The waveguide measurement device connected to network analyzer (Agilent E5071A) was used to measure the EMI SE of as-prepared composites films as a function of number of RGO layers. The densities of RGO and PEI were measured by pycnometer apparatus (AccuPyc 1330) at room temperature.

RESULTS AND DISCUSSION

Figure 3 schematically shows the fabrication procedure of a single [RGO/PEI] layer. The RGO layer was deposited on the SS plate by an anodic EPD (Figure 3A,B) followed by the q-PEI deposition by cathodic EPD on the top (Figure 3C). The fabricated [PEI/RGO] bilayer was thermally reimidized (Figure 3D). Then, using a Scotch tape attached over the edge of the PEI film (Figure 3E), the [PEI/RGO] layer was mechanically detached (Figure 3E,F) with ease. As seen in the digital image of the detached PEI/RGO bilayer film (Figure 3F), the film is transparent and flexible.

Using the fabricated [PEI/RGO] films, the [PEI/RGO/PEI/RGO/PEI] interleaved structure was fabricated, as schematically seen in Figure 4. Two as-prepared [PEI/RGO] films with one adhesive PEI film inserted between these two were compression molded. As seen in the digital image of the resulting film, the resulting double-PEI/RGO film, [PEI/RGO/PEI/RGO/PEI], is also flexible and transparent.

The EMI SE can be defined as a measure of the attenuation in the electromagnetic field strength at a point in space resulted from the insertion of a shielding material. In the EMI shielding theory, the absorbance (A), reflectance (R), and transmittance (T) represent the magnitudes of an absorbed wave, reflected wave, and transmitted wave, respectively, by the shield. The total incident power can be expressed as sum of A, R, and T or expressed as $1 = A + R + T$,[37] where the value 1 represents the whole incident wave intensity. When an electromagnetic (EM) wave passes through a conductive material, its amplitude decreases exponentially due to ohmic losses. And the skin depth is the distance for the wave to be attenuated to 1/e (37%) of its incident EM wave, which can be defined by the equation[38] as follows:

$$\text{skin depth } (\delta) = \frac{1}{\sqrt{\pi \mu \sigma f}} \quad (2)$$

where μ and σ are respectively, magnetic permeability and electrical conductivity of shielding material and f is frequency. The total EMI SE can be written as SE = 10 log (P_{in}/P_{out}),[39] where P_{in} and P_{out} are the power incident on and transmitted through a shielding material. By substituting $P_{out} = P_{in}\, e^{-t/\delta}$ to the previously written equation, where t is thickness of the

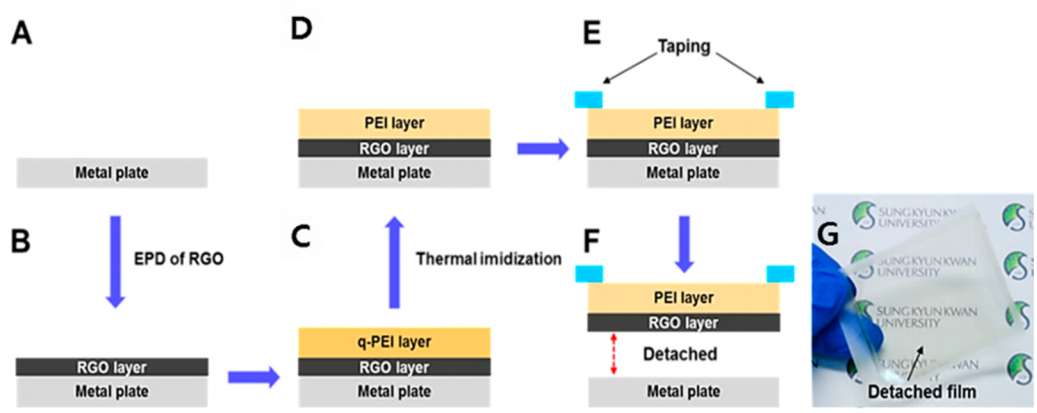

Figure 3. Schematic of PEI/RGO bilayer film fabrication. SS plate (A), RGO layer deposited on SS plate (B), q-PEI deposited on RGO (C), PEI/RGO after thermal reimidization (D), scotch tape attached on the rim (E,F), and digital image of mechanically detached bilayer [PEI/RGO] film (G).

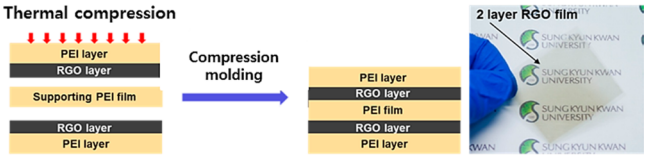

Figure 4. Schematic of double-PEI/RGO film fabrication. [PEI/RGO/PEI/RGO/PEI] film fabricated by compression molding, also exhibiting the digital image of the resulting film.

shielding material, finally we can get the simplified SE_A (absorption loss) equation[38] as follows:

$$SE_A = 20 \log(e^{t/\delta}) = 8.69\left(\frac{t}{\delta}\right) \quad (3)$$

As it is clearly shown in eqs 2 and 3, the SE_A is inversely proportional to the number of skin depth, but proportional to the thickness of the shielding material. In other words, with increasing μ and σ values of shielding material, the higher shielding performance can be achieved. Furthermore, the dominant mechanism of the EMI shielding of the graphene attributed to SE was reported to be absorption rather than reflection.[2]

The other shielding mechanism is called reflectance, which occurs from the difference between the value of shield impedance (Z_s) and air impedance (Z_0). The SE_R (reflection loss) equation[38] can be written as follows:

$$SE_R = 90.5 + 10 \log\left(\frac{\sigma}{\mu_r f}\right) \quad (4)$$

Here in eq 4, we can notice that contrary to eqs 2 and 3, the μ_r (relative magnetic permeability) of shielding material is inversely proportional to number of SE_R but, only proportional to σ. However, due to the difficulty in a direct measurement of the EMI SE, SE is quantitatively expressed as S-parameters that represent the scattering of the wave. The scattering parameters S11 and S21 are coefficients indicating the amount of electromagnetic reflection and transmission, respectively. In the measurement using a vector network analyzer, the measured S11 and S21 of a two-port network analyzer are used to calculate the reflectance and transmittance values as $R = |S11|^2$ and $T = |S21|^2$, respectively. Furthermore, the absorbance can be subsequently calculated by the equation $A = 1 - R - T$.[12] In the measured S21, or the transmittance (T) of the shield SE can be expressed as follows:

$$SE\ (dB) = -10 \log_{10}|T| \quad (5)$$

where $T = |S21|^2$.

Figure 5A shows the surface morphology of the RGO film as deposited on the SS plate. It can be seen that the RGO sheets are packed on the top, exhibiting the edges of the RGO sheets. Figure 5B shows the PEI layer deposited on the top of the RGO layer through the alternating EPD process. The PEI surface looks smooth and defect free. Figure 5C,D (the same images at different magnifications) represents the cross section images of the RGO layer placed on the top of the PEI layer. The image of the RGO surface is the detached one from the SS plate (see Figure 3F,G). The cross-sectional morphology of [PEI/RGO/PEI] (single-PEI/RGO) and [PEI/RGO/PEI/RGO/PEI] multilayer (double-PEI/RGO) films were examined by TEM (Figures 5 C-E). It can be clearly seen that the RGO layer is less than 20 nm. Figure 5E shows the cross-section of the double-PEI/RGO film exhibiting two RGO layers, which is very thin, interleaved in the PEI layers, ca. 2 μm. Also, significant void and interlaminar delamination could not be observed at the interfaces of PEI and RGO layer.

Figure 5F shows Raman spectra of pristine graphite powder and RGO film prepared by the EPD technique. The D-band at 1343 cm^{-1} and a G-band around 1588 cm^{-1} appear in the spectra, indicating sp^3 hybridization of carbon atoms during the oxidation from graphite and the recovery of hexagonal network of carbon atoms with defects.[30] The intensity ratio of D- and G-band (I_D/I_G) provides a sensitive measure of the disorder and crystallite size of the graphitic layers. The I_D/I_G of graphite powder and RGO were, respectively 0.07 and 1.25. The D-band intensity in the RGO film was found to be higher than the G-band compared to graphite, which indicates remaining structural defects and disorder in RGO resulted from the oxidation and reduction process. The oxygen-functional groups are released as CO and CO_2, inducing more defects in the carbon backbone and causing the I_D/I_G increase from 0.07 to 1.25. In addition, the intensity of 2D (2686 cm^{-1}) peaks decreased in the Raman spectra of RGO, as a result of oxidation and reduction process.[30]

It should be underlined that the delamination issue in PEI/RGO film is crucial, particularly, in the layered structures of graphene. When the negatively charged q-PEI emulsions move

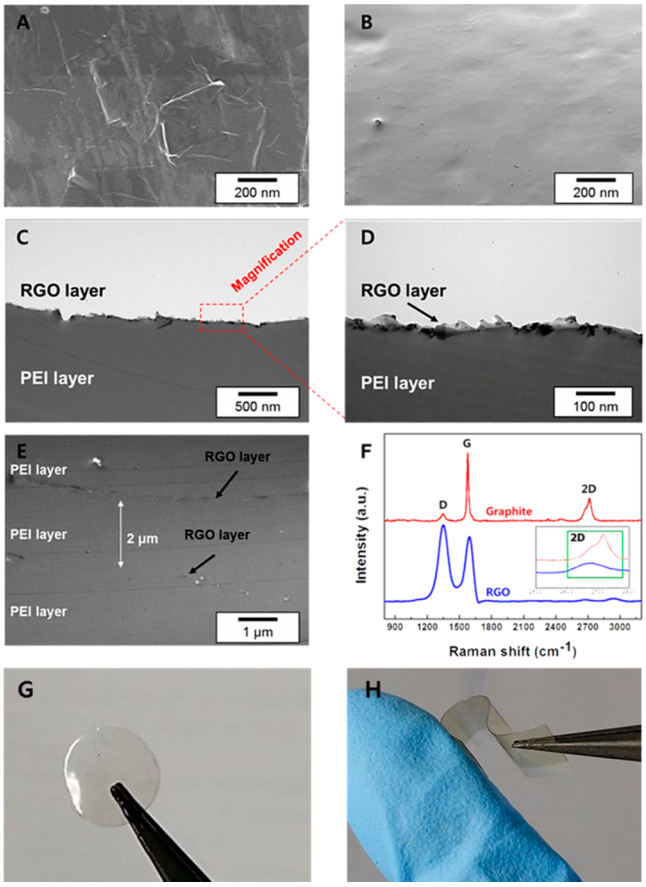

Figure 5. SEM images of RGO surface (A), q-PEI surface coated on RGO (B), TEM images of PEI layer deposited on RGO at different magnifications (C), and (D) also exhibiting cross-section of two RGO layers inserted in fabricated [PEI/RGO/PEI/RGO/PEI] film (E). Raman spectra of pristine graphite powder (red) and RGO film (blue) prepared by the EPD method (F). Digital images of single-PEI/RGO film after scissors cutting (G) and double-PEI/RGO film under bending (H) demonstrating robustness of films against delamination.

toward on the previously deposited RGO sheets during the cathodic EPD process, the water medium allows good wetting of q-PEI drops and ensures their facile infiltration into the RGO sheets under the strong electrophoretic squeezing force in EPD,[31,35] which could facilitate cohesive flocculation and the strong physical anchoring between PEI and RGO. As a result, no delamination was observed in our PEI/RGO multilayer films.

Figure 5G,H shows the fabricated PEI/RGO composite films cut by scissors as a circular shape (7 mm in diameter) for EMI testing (Figure 5G) and bent in high curvature by hands. It is demonstrated that our multilayer film has such a strong interlaminar strength that the fabricated films could sustain fairly high external stresses by cutting and bending.

The volume fractions of RGO in the single- and double-PEI/RGO films were measured as 0.49 ± 0.02 and 0.66 ± 0.02%, respectively, where ρ_f and ρ_m were 2.35 and 1.27 g/cm^3, respectively. The SE value of our PEI/RGO composite films were achieved by using an extremely small amount of RGO <0.66 vol %, which ensures the flexibility and transparency (see Table 1 and Figure 5G,H).

The light transmittance for both [PEI/RGO/PEI] and [PEI/RGO/PEI/RGO/PEI] films is shown in Figure 6 and Table 1. The conductivity of the RGO film fabricated by EPD was 1.25 × 10^3 S/m. We could see that the optical transparency of the film gradually decreased with increasing thickness or number of RGO layers. As-prepared films exhibit a transparency of up to 73 and 62% for the single-PEI/RGO ([PEI/RGO/PEI]) and double-PEI/RGO ([PEI/RGO/PEI/RGO/PEI]) films, respectively (see Table 1 and Figures 3G and 4). Although the transparency gradually decreased with the increasing number of RGO layers, the [PEI/RGO/PEI/RGO/PEI] film still exhibited the optical transparency up to 62%. In addition, it was observed that in ultraviolet area PEI and single- and double-PEI/RGO films demonstrated the UV blocking performance, as shown in Figure 6.

Table 1. Electrical Conductivity and Light Transmittance of Pristine PEI, Single-PEI/RGO, and Double-PEI/RGO

sample name	conductivity (S/m)	light transmittance (%)	number of RGO films (20 nm)	ν_{RGO} (%)	SE (dB)
pristine PEI	0	87	0	0	0
single-PEI/RGO	1.25 × 10^3	73	1	0.49	3.09
double-PEI/RGO	1.25 × 10^3	62	2	0.66	6.37

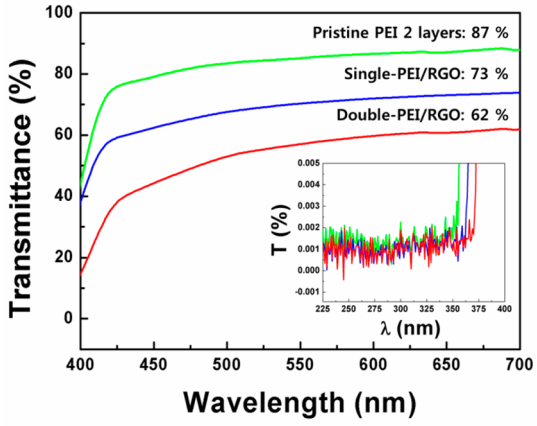

Figure 6. Light transmittance of two layers of pristine PEI (green line), single-PEI/RGO (blue line), and double-PEI/RGO (red line) films.

Figure 7A demonstrates the basic mechanism of EMI shielding by RGO. Figure 7B–D shows that the absolute values of absorbance and reflectance increase with the number of RGO layers. However, the relative contributions of each component to the total shielding vary according the number of RGO layers. For single-PEI/RGO and double-PEI-RGO, approximately 92 and 96% of shielding out of 3.09 and 6.37 dB was achieved by absorption, and in comparison with reflectance, the significant increase by absorbance in the shielding was observed, especially in double-PEI/RGO (Figure 7B). The average SE values of PEI, single-PEI/RGO, and double-PEI/RGO were 0, 3.09, and 6.37 dB, respectively, over a frequency range of 0.5–8.5 GHz. The SE increased almost linearly with the number of RGO layers in as-prepared composites films (Figure 7F). In this work, for the single-PEI/RGO and double-PEI/RGO, the average rates of *R*, *A*, and *T* were 0.012, 0.1379, 0.8501 and 0.02, 0.4826, 0.4974 over a frequency range of 0.5–8.5 GHz, respectively. These results

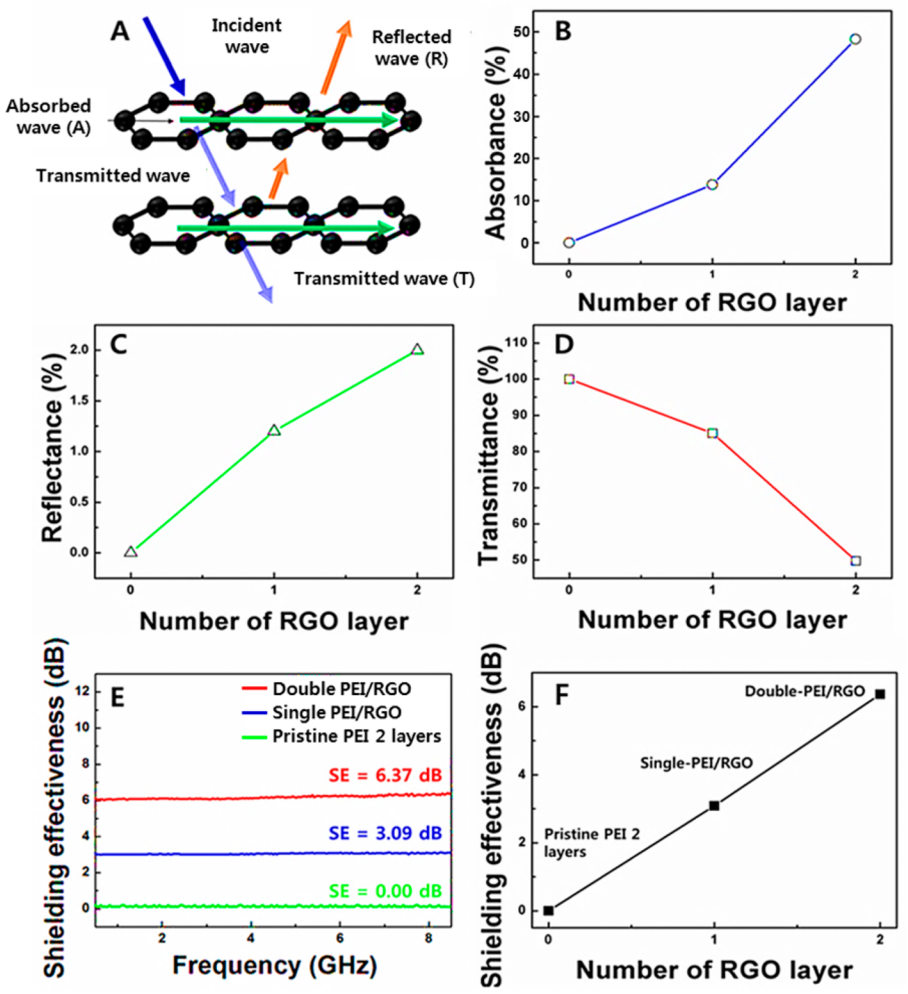

Figure 7. Description of wave dispersion on RGO film (A), the percentage of average contribution of RGO on SE by absorbance (B), reflectance (C), and decrease in transmittance resulted from EMI shielding by RGO (D). Comparison of SE value of films with different number of RGO layers, respectively 0, 1, and 2 (E and F).

indicate that the SE approximately up to 50% of incident waves could be achieved by the double-PEI/RGO film.

CONCLUSIONS

The fabrication technique of PEI/RGO film was developed by an alternating anodic and cathodic EPD particularly at a low voltage (less than 10 V). The single- and double-PEI/RGO films with 0.49 and 0.66 vol %, respectively, were successfully fabricated. Our RGO interleaved PEI/RGO film fabrication technique allowed the maximized EMI shielding performance of graphene materials. The results of EMI SE of single- and double-PEI/RGO films were 3.09 and 6.37 dB, respectively, while retaining light transparency up to 73 and 62%, resulting from their unique interleaved structure composed of 20 nm RGO thin films. Finally, the delamination was not observed even after the annealing process and during or after the cutting and detaching processes. We believe that this newly developed RGO interleaved structure can have practical applications in various fields including EMI shielding, touch screen, displays, portable electronic devices, and transparent electronics.

AUTHOR INFORMATION

Corresponding Author

*J.-D. Nam. E-mail: jdnam@skku.edu. Tel: +82-31-290-7285. Fax: +82-31-292-8790.

Author Contributions

This paper was written through contributions of all authors.

Notes

The authors declare no competing financial interest.

ACKNOWLEDGMENTS

This research was supported by the research grants (2012M1A2A2671788, 2013M3C8A3078512, and 2011-0031643) through the National Research Foundation of Korea (NRF) funded by the Ministry of Education, Science and Technology. This work was partly supported by the GRRC program of Gyeonggi province.

REFERENCES

(1) Liang, J.; Wang, Y.; Huang, Y.; Gao, H.; Chen, Y. Electromagnetic Interference Shielding of Graphene/Epoxy Composites. *Carbon* **2009**, *47*, 922−925.

(2) Chung, D. D. L. Electromagnetic Interference Shielding Effectiveness of Carbon Materials. *Carbon* **2001**, *39*, 279−285.

(3) Hu, M.; Gao, J.; Dong, Y.; Li, K.; Shan, G.; Yang, S.; Li, R. K. Flexible Transparent PES/Silver Nanowires/PET Sandwich-Structured Film for High-Efficiency Electromagnetic Interference Shielding. *Langmuir* **2012**, *28*, 7101−7106.
(4) Funkenbusch, A. W.; Bright, C. I. Fleming, R. J. Durable Transparent EMI Shielding Film. U.S. Patent 6,818,291, Nov 16, 2004.
(5) Kim, K. S.; Ahn, J. H.; Kim, P.; Hong, B. H. Large-Scale Pattern Growth of Graphene Films for Stretchable Transparent Electrodes. *Nature* **2009**, *457*, 706−710.
(6) Lee, S. K.; Kim, B. J.; Ahn, J. H. Stretchable Graphene Transistors with Printed Dielectrics and Gate Electrodes. *Nano Lett.* **2011**, *11*, 4642−4626.
(7) Singh, A. P.; Gupta, B. K.; Dhawan, S. K. Multiwalled Carbon Nanotube/Cement Composites with Exceptional Electromagnetic Interference Shielding Properties. *Carbon* **2013**, *56*, 86−96.
(8) Singh, A. P.; Mishra, M.; Chandra, A.; Dhawan, S. K. Graphene Oxide/Ferrofluid/Cement Composites for Electromagnetic Interference Shielding Application. *Nanotechnology* **2011**, *22*, 9.
(9) Yamada, T.; Morizane, T.; Arimitsu, T.; Miyake, A.; Makino, H.; Yamamoto, N.; Yamamoto, T. Application of Low Resistivity Ga-Doped ZnO Films to Transparent Electromagnetic Interference Shielding Material. *Thin Solid Films* **2008**, *517*, 1027−1031.
(10) Niu, Y. Electromagnetic Interference Shielding with Polyaniline Nanofibers Composite Coatings. *Polym. Eng. Sci.* **2008**, *48*, 355−359.
(11) Jung, B.; Kwon, Y. R.; Ko, J. M.; Kim, M. S.; Cho, S. H.; Lee, J. Y.; Joo, J. PET Fabric/Poly(3,4-ethylenedioxythiophene) Composite with High Electrical Conductivity for EMI Shielding. *Mol. Cryst. Liq. Cryst.* **2006**, *464*, 109−117.
(12) Hong, S. K.; Kim, K. Y.; Cho, B. J. Electromagnetic Interference Shielding Effectiveness of Monolayer Graphene. *Nanotechnology* **2012**, *23*, 5.
(13) Kim, B. R.; Lee, H. K.; Kim, E. M.; Lee, S. H. Intrinsic Electromagnetic Radiation Shielding/Absorbing Characteristics of Polyaniline-Coated Transparent Thin Films. *Synth. Met.* **2010**, *160*, 1838−1842.
(14) Choi, Y. J.; Gong, S. C.; Johnson, D. C.; Golledge, S.; Yeom, G. Y.; Park, H. H. Characteristics of the Electromagnetic Interference Shielding Effectiveness of Al-Doped ZnO Thin Films Deposited by Atomic Layer Deposition. *Appl. Surf. Sci.* **2013**, *269*, 92−97.
(15) Qiu, J. D.; Wang, G. C.; Liang, R. P.; Xia, X. H.; Yu, H. W. Controllable Deposition of Platinum Nanoparticles on Graphene as an Electrocatalyst for Direct Methanol Fuel Cells. *J. Phys. Chem. C* **2011**, *115*, 15639−15645.
(16) Kim, K. S.; Zhao, Y.; Jang, H.; Lee, S. Y.; Kim, J. M.; Kim, K. S.; Ahn, J. H.; Kim, P.; Choi, J. Y.; Hong, B. H. Large-Scale Pattern Growth of Graphene Films for Stretchable Transparent Electrodes. *Nature* **2009**, *457*, 706−710.
(17) Wang, G.; Yang, J.; Park, J.; Gou, X.; Wang, B.; Liu, H.; Yao, J. Facile Synthesis and Characterization of Graphene Nanosheets. *J. Phys. Chem. C* **2008**, *112*, 8192−8195.
(18) Xu, C.; Wang, X.; Zhu, J. Graphene-Metal Particle Nanocomposites. *J. Phys. Chem. C* **2008**, *112*, 19841−19845.
(19) Liang, J.; Wang, Y.; Huang, Y.; Ma, Y.; Liu, Z.; Cai, J.; Zhang, C.; Gao, H.; Chen, Y. Electromagnetic Interference Shielding of Graphene/Epoxy Composites. *Carbon* **2009**, *47*, 922−925.
(20) Yan, D. X.; Ren, P. G.; Pang, H.; Fu, Q.; Yang, M. B.; Li, Z. M. Efficient Electromagnetic Interference Shielding of Lightweight Graphene/Polystyrene Composite. *J. Mater. Chem.* **2012**, *22*, 1872−18774.
(21) Zhang, H. B.; Zheng, W. G.; Yan, Q.; Jiang, Z. G.; Yu, Z. Z. The Effect of Surface Chemistry of Graphene on Rheological and Electrical Properties of Polymethylmethacrylate Composites. *Carbon* **2012**, *14*, 5117−5125.
(22) Hwang, E. H.; Sarma, S. D. Acoustic Phonon Scattering Limited Carrier Mobility in Two-Dimensional Extrinsic Graphene. *Phys. Rev. B: Condens. Matter Mater. Phys.* **2008**, *77*, 6.
(23) Hwang, T.; Oh, J. S.; Hong, J. P.; Nam, G. Y.; Bae, A. H.; Son, S. I.; Lee, G. H.; Sung, H. K.; Lee, Y.; Nam, J. D. One-Step Metal Electroplating and Patterning on a Plastic Substrate Using an Electrically-Conductive Layer of Few-Layer Graphene. *Carbon* **2012**, *50*, 612−621.
(24) Park, S.; Ruoff, R. S. Chemical Methods for the Production of Graphenes. *Nat. Nanotechnol.* **2009**, *4*, 217−224.
(25) Bae, S. K.; Kim, H. K.; Lee, Y. B.; Xu, X.; Park, J. S.; Zheng, Y.; Balakrishnan, J.; Lei, T.; Kim, H. R.; Song, Y. I.; Kim, Y. J.; Kim, K. S.; Ozyilmaz, B.; Ahn, J. H.; Hong, B. H.; Iljima, S. Roll-To-Roll Production of 30-Inch Graphene Films for Transparent Electrodes. *Nat. Nanotechnol.* **2010**, *5*, 574−578.
(26) Tung, V. C.; Allen, M. J.; Yang, Y.; Kaner, R. B. High-Throughput Solution Processing of Large-Scale Graphene. *Nat. Nanotechnol.* **2009**, *4*, 25−29.
(27) An, S. J.; Zhu, Y.; Lee, S. H.; Stoller, M. D.; Emilsson, T.; Park, S.; Velamakanni, A.; An, J.; Ruoff, R. S. Thin Film Fabrication and Simultaneous Anodic Reduction of Deposited Graphene Oxide Platelets by Electrophoretic Deposition. *J. Phys. Chem. Lett.* **2010**, *1*, 1259−1263.
(28) Neirinck, B.; Fransaer, J.; Biest, O.; Vleugels, J. Aqueous Electrophoretic Deposition in Asymmetric AC Fields (AC-EPD). *Electrochem. Commun.* **2009**, *11*, 57−60.
(29) Ghosh, T.; Biswas, C.; Oh, J. S.; Arabale, G.; Hwang, T.; Luong, D. L.; Jin, M.; Lee, Y. H.; Nam, J. D. Solution-Processed Graphite Membrane from Reassembled Graphene Oxide. *Chem. Mater.* **2012**, *24*, 594−599.
(30) Wang, M.; Oh, J. S.; Ghosh, T.; Hong, S.; Nam, G.; Hwang, T.; Nam, J. D. An Interleaved Porous Laminate Composed of Reduced Graphene Oxide Sheets and Carbon Black Spacers by in Situ Electrophoretic Deposition. *RSC Adv.* **2014**, *4*, 3284.
(31) Kim, S. H.; Oh, J. S.; Hwang, T.; Cho, M.; Lee, Y. K.; Choi, H. R.; Kim, S. W.; Nam, J. D. Low-Voltage Electrophoretic Deposition of Polyetherimide Through Quarternization and Re-Imidization Reactions. *Kor.−Aust. Rheol. J.* **2013**, *25*, 261−266.
(32) Oh, J. S.; Kim, S. H.; Hwang, T.; Kwon, H. Y.; Lee, T. H.; Bae, A. H.; Choi, H. R.; Nam, J. D. Laser-Assisted Simultaneous Patterning and Transferring of Graphene. *J. Phys. Chem. C* **2013**, *117*, 663−668.
(33) Sarkar, P.; Nicholson, P. S. Electrophoretic Deposition (EPD): Mechanisms, Kinetics, and Application to Ceramics. *J. Am. Ceram. Soc.* **2005**, *79*, 1987−2002.
(34) Chen, Y.; Zhang, X.; Yu, P.; Ma, Y. Electrophoretic Deposition of Graphene Nanosheets on Nickel Foams for Electrochemical Capacitors. *J. Power Sources* **2010**, *195*, 3031−3035.
(35) Besra, L.; Liu, M. A Review on Fundamentals and Applications of Electrophoretic Deposition. *Prog. Mater. Sci.* **2007**, *52*, 1−61.
(36) Vasileiou, A. A.; Kontopoulou, M.; Docoslis, A. A Noncovalent Compatibilization Approach to Improve the Filler Dispersion and Properties of Polyethylene/Graphene Composites. *ACS Appl. Mater. Interfaces* **2014**, *6*, 1916−1925.
(37) Zhang, H. B.; Yan, Q.; Zheng, W. G.; He, Z.; Yu, Z. Z. Tough Graphene-Polymer Microcellular Foams for Electromagnetic Interference Shielding. *ACS Appl. Mater. Interfaces* **2011**, *3*, 918−924.
(38) Skinner, H.; Slattery, K. *Platform Interference in Wireless Systems: Models, Measurement, and Mitigation*; Newnes: Oxford, U. K., 2008; Chapter 8, pp 256−267.
(39) Maiti, S.; Shrivastava, N. K.; Suin, S.; Khatua, B. B. Polystyrene/MWCNT/Graphite Nanoplate Nano Composites: Efficient Electromagnetic Interference Shielding Material Through Graphite Nanoplate-MWCNT-Graphite Nanoplate Networking. *ACS Appl. Mater. Interfaces* **2013**, *5*, 4712−4724.